Structural Origin of Selectivity in Class II-Selective Histone Deacetylase Inhibitors

Guillermina Estiu,[†] Edward Greenberg,[‡] Christopher B. Harrison,[†] Nicholas P. Kwiatkowski,[‡] Ralph Mazitschek,[‡] James E. Bradner,[‡] and Olaf Wiest*,[†]

Walther Cancer Research Center and Department of Chemistry and Biochemistry, University of Notre Dame, Notre Dame, Indiana 46556-5670, and Broad Institute of Harvard University and MIT, 7 Cambridge Center, Cambridge, Massachusetts 02142

Received December 7, 2007

The development of class- and isoform-selective histone deacetylase (HDAC) inhibitors is highly desirable for the study of the complex interactions of these proteins central to transcription regulation as well as for the development of selective HDAC inhibitors as drugs in epigenetics. To provide a structural basis for the rational design of such inhibitors, a combined computational and experimental study of inhibition of three different histone deacetylase isoforms, HDAC1, -6, and -8, with three different hydroxamate inhibitors is reported. While SAHA was found to be unselective for the inhibition of class I and class II HDACs, the other inhibitors were found to be selective toward class II HDACs. Molecular dynamics simulations indicate that this selectivity is caused by both the overall shape of the protein surface leading to the active site and specific interactions of an aspartate residue in a polar loop and two phenylalanines and a methionine in a nonpolar loop. Monitoring the specific interactions as a function of the simulation time identifies a key sulfur$-\pi$ interaction. The implications of the structural motifs for the design of class II-selective HDAC inhibitors are discussed.

Introduction

Remodeling of chromatin has a key role in epigenetic regulation of gene expression and is crucial to the onset and progression of cancer.[1,2] Chromatin modification is tightly regulated by the opposing activities of histone acetyltransferases (HATs[a]) and histone deacetylases (HDACs). Whereas HATs transfer acetyl groups to amino-terminal residues in histones, HDACs catalyze the removal of acetyl groups from lysine residues, leading to chromatin condensation and transcriptional repression.[3–5]

In recent years, inhibition of HDAC has emerged as a promising strategy to reverse aberrant epigenetic changes associated with cancer and several other diseases, and several classes of HDAC inhibitors (HDACi) have been found to have potent anticancer activity in preclinical studies, with remarkable tumor specificity.[6,7] Furthermore, it has become apparent that in addition to their intrinsic effects in tumor cells, HDACi might also affect neoplastic growth and survival by regulating host immune response and tumor vasculature.[3,8–10] As a result, numerous HDAC inhibitors have entered clinical studies and the first-in-class drug suberoylanilide hydroxamic acid (SAHA) was approved by the FDA in 2006 for the treatment of cutaneous T-cell lymphoma.

Eighteen HDACs have been identified in humans and subdivided into four classes on the basis of their homology to yeast HDACs, their subcellular localization, their enzymatic activities, and a phylogenetic analysis.[5,11] There is experimental evidence that different subtypes have intrinsic differences in substrate selectivity.[12–15] To develop the tools for more detailed studies of individual isoforms and to avoid the risk of toxicity due to lack of selectivity, research is focused toward the development of isoform-specific HDACi's. Whereas some class I-selective inhibitors with nanomolar activity have been developed,[3,13–16] only a few class II-selective inhibitors are known. High-throughput screening of a large library identified the class II-selective HDACi tubacin, which induces hyperacetylation of α-tubulin and has no effect on histone acetylation status.[13] This is consistent with the notion that HDAC6 (a member of class IIb) has unique substrate specificity for the α-tubulin deacetylase domain of the cytoskeletal protein α-tubulin. In addition to being implied in tumor progression, HDAC6 is present in Lewy bodies associated with neurodegenerative disorders, such as Parkinson's disease and dementia, regulating various processes in the cytoplasm.[17]

Understanding the structural origin of selectivity is the basis for a rational design of isoform-selective HDACi with increased potency. To this end, we have studied the interactions in the active site of class I and class II HDACs that stabilize SAHA, tubacin, and its close analogue **1** (NK308).[18] The structures of the ligands studied are shown in Figure 1. Using the widely accepted pharmacophore that divides HDAC inhibitors into metal binding moiety, linker, and cap region, the ligands shown all belong to the hydroxamate class of inhibitors, sharing the same Zn-binding group and link region. As will be discussed in detail later, the differences responsible for selectivity are concentrated in the cap region that interacts with the surface area of the active site.

Complexation of the hydroxamic ligands involves chelation of the hydroxamic acid or hydroxamate group to the Zn^{2+} ion of the histone deacetylases active site. Two aspartates and one histidine residue complete the first coordination sphere of the metal center. The ligand is further stabilized by two additional His in the second coordination sphere, which establish hydrogen bond interactions with the oxygens and nitrogen of the hydroxamic group. There is little direct experimental evidence regarding the protonation state of the hydroxamic acid and the His residue hydrogen bonded to it, but computational studies from our group[19] and others[20] indicate a negative hydroxamate and

* To whom correspondence should be sent. Phone: (574) 631 5876. Fax: (574) 631 6652. E-mail: owiest@nd.edu.

[†] University of Notre Dame.

[‡] Broad Institute of Harvard University and MIT.

[a] Abreviations: HAT, histone acetyltransferase; HDAC, histone deacetylase; HDLP, histone deacetylase-like protein; HDLP, archeobacterial homologue of eukaryotic deacetylases; SAHA, suberoyl anilide hydroxamic acid.

10.1021/jm7015254 CCC: $40.75
Published on Web 04/16/2008

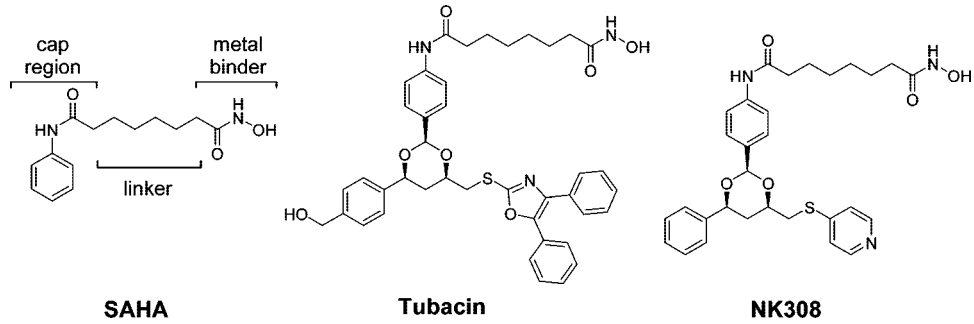

Figure 1. HDAC inhibitors studied.

a protonated His give geometries very close to the ones observed experimentally.[21,22] This protonation scheme is favored by coordination of the His residues of the outer sphere to Asp residues (Asn in class II), defining a charge relay system that polarizes the imidazole Nϵ and increases its basicity. The Zn^{2+} ion is located at the bottom of a tunnel (11 Å deep in HDLP) that accommodates the linker region of the ligand and provides additional stabilization through hydrophobic interactions. This region of the protein is highly conserved across the different HDAC families, and it is difficult to envision interactions in the active site that would be able to distinguish different isoforms.[21,23]

The cap region of the different inhibitors shown in Figure 1 can be oriented toward several distinct pockets in the solvent-exposed entrance of the channel that are less conserved across the different isoforms. In addition, the existence of a second pocket close to the active site, which is believed to be involved in product release,[23] has to be considered. This tube-like pocket has a different shape in HDAC6[22] and HDAC8[21,23] and has been found to be occupied by TSA in a HDAC8 inhibitor complex.[23a,b]

Although isoform selectivity has been widely acknowledged as a goal in the development of novel HDAC inhibitors that might untangle the role of the individual HDACs in gene translation and might be useful for the treatment of a wide range of cancer and noncancer diseases, enzyme assay data for the inhibition of the individual isoforms have only recently started to be available due to the lack of isoform-pure proteins. In addition, there is even less structural work to shed light on the interactions responsible for such selectivity. In particular, there are at this point no experimental structures of class II HDACs with isoform-selective inhibitors available. We therefore used a combined experimental and computational approach to determine the degree and structural origin of the selectivity of the first-in-class, FDA-approved HDAC inhibitor SAHA and a series of novel inhibitors developed by some of us. We will first present the results of isoform-specific enzyme assays that demonstrate selectivity of some known and novel inhibitors toward HDAC1, -6, and -8. The structural origin of these experimentally observed selectivities and lack of selectivity for SAHA will be analyzed using MD simulations on the 10 to 40 ns time scale. Finally, we will discuss the implications of the interactions observed in the simulations for the design of novel and specific HDAC inhibitors.

Computational and Experimental Methods

Construction of Enzyme Models. There is currently no structure for human HDAC6 or any other class IIb HDAC available. A homology model of HDAC6 was thus constructed using the 38% sequence alignment between the bacterial HDAC6 homologue FB188 HDAH and the AAH13773.1 *Homo sapiens* HDAC6 from BLASTp.[24] The C-terminus (residues 500−783 of the resulting alignment) and the X-ray structure of HDAH [pdb 1zz1.pdb] were used to generate a series of 10 homology models using Modeller4.0.[25] Subsequent minimization of the individual models was used and resulted in backbone convergence and consistent models derived from the 10 homology models. Comparative Ramachandran calculations[26] of the HDAH and HDAC6 structures indicated no increase of residues in disallowed regions and a 1.2% increase in generously allowed regions for the HDAC6 homology model. Structural fitting of the HDAH and the HDAC6 model using the McLachlan algorithm[27] indicated a 0.78 rmsd of the alpha carbons. Although the MD refinement of homology models is a question of ongoing debate, the methodology used here relies on extensive MD simulations of the enzyme−inhibitor complexes. The HDAC6 model was therefore further refined through consecutive MD minimizations, and progressively releasing constraints from the hydrogen, side chain, and backbone atoms using Amber8.0. MD equilibration at 300 K over 500 ps using NVT conditions was followed by simulated sequence annealing consisting of an increase of the temperature to 400 K over 150 ps, high-temperature sampling for 300 ps, and gradual cooling to 300 K over 150 ps. A subsequent 250 ps NVT equilibration was followed by 1 ns of NPT equilibration. This extensive minimization, simulated annealing, and equilibration protocol was considered necessary to adequately sample and equilibrate the homology model due to the number of high-energy atomic contacts in the initial structure. The homology model of HDAC1 was constructed in a similar manner and was described earlier.[21]

The crystallographic structure of human HDAC8 (class I) complexed with hydroxamic inhibitors has been determined with resolutions of 1.9 A (TSA), 2.3 A (MS-344), 2.9 A (SAHA), and 2.2 A (CRA-19156) (pdb codes 1T64, 1T67, 1T69, and 1VKG, respectively). Because no structural information is available for the tubacin complex, we built the initial geometry by substitution of the MS-344 ligand by tubacin in the structure from the pdb file 1T67. The same procedure was applied to build the initial structures of the complex of HDAC8 and **1**.

Molecular Dynamics Simulations. Initial coordinates for the protein atoms were taken from the crystallographic structure of human HDAC8 and the homology model of HDAC6 and HDAC1. The ionizable residues were set to their normal ionization states at pH 7, except for the His residue H-bond coordinated to the negative end of the hydroxamate ligand, which has been modeled as positively charged. The protein atoms, as well as all the water molecules of the crystal structure, were surrounded by a periodic box of TIP3P[28] water molecules that extended 10 Å from the protein. Na^+ counterions were placed by LEaP[29] to neutralize the system.

The ff02 version[30] of the all-atom AMBER force field was used, together with GAFF,[31] to model the system. Atom-centered partial charges were derived by using the AMBER antechamber program (RESP methodology),[32] after geometry optimization at the B3LYP/6-31G* level. Solvent molecules and counterions were initially relaxed by means of energy minimizations. The full system was then minimized to remove bad contacts in the initial geometry. All MD simulations were carried out using the SANDER version

Table 1. K_i of Inhibitors Studied in HDAC1, -6, and -8

	HDAC1 (nM)	HDAC6 (nM)	HDAC8 (nM)
SAHA	48	21	2000
tubacin	995	142	6300
1	88	28	6100

included in the AMBER 8.0 suite of programs.[33] The time step was chosen to be 1.5 fs, and the SHAKE algorithm[34] was used to constrain all bonds involving hydrogen atoms. A nonbonded cutoff of 10.0 Å was used, and the nonbonded pair list was updated every 25 time steps. The pressure (1 atm) and the temperature (300 K) of the system were controlled during the MD simulation by Berendsen's method.[35] Periodic boundary conditions were applied to simulate a continuous system. To include the contributions of long-range interactions, the particle-mesh-Ewald (PME) method[36] was used with a grid spacing of ~1 Å combined with a fourth-order B-spline interpolation to compute the potential and forces in between grid points.

For all the configurations that were examined, at least 10 ns trajectories were computed after equilibration and coordinates were saved every 250 time steps. The trajectories were analyzed using the PTRAJ module of AMBER.

Enzyme Assays. To assess the effect of tubacin, SAHA, and **1** on histone deacetylase enzyme function *in vitro,* we performed a dose-ranging study in full-length HDAC1 (BPS Bioscience), HDAC6 (Takeda Pharmaceuticals), and HDAC8 (Upstate 14-609) using a fluorometric assay (Upstate 17-372). In brief, HDAC1 (3.3 μg/mL), HDAC6 (0.5 μg/mL), or HDAC8 (1 μg/mL) was incubated with one or two concentrations of a commercially available fluorophore-conjugated substrate (6 μM for HDAC1, 12.5 and 25 μM for HDAC6, 25 and 50 μM for HDAC8; Upstate 12-512). Reactions were carried out in HDAC assay buffer (50 mM HEPES, 100 mM KCl, 0.001% Tween-20, 0.05% BSA, pH 7.4). Quantitative measurements were obtained in real time on a Varioskan microplate reader (Thermo), in the presence of increasing concentrations of the inhibitor. Data were normalized to a control reaction in the presence of an equal volume of DMSO. Each measurement represents the arithmetic mean of three independent experiments. Increasing concentrations of all compounds resulted in a dose-dependent inhibition of HDAC1, HDAC6, and HDAC8.

Results and Discussion

We started our investigation by determining the inhibition of three different isoforms by SAHA, **1**, and tubacin. Table 1 summarizes the K_i values for SAHA, **1**, and tubacin in HDAC1, -6, and -8. In agreement with earlier studies, SAHA is found to be fairly unselective with essentially equal potency against HDAC1, a member of the class I, and the class II HDAC6. It is noteworthy that the K_i for the inhibition of HDAC8 is approximately 100 times higher. This result was unexpected and is in contrast to the results by Etzkorn and co-workers,[37] who found an IC_{50} of 270 nM for the inhibition of recombinant HDAC8 by SAHA, but in line with more recent studies of SAHA[38] as well as the finding that HDAC8 is evolutionary divergent from other class 1 HDACs as well as a series of biochemical studies that point to the uniqueness of HDAC8.[39] Tubacin, on the other hand, is found to be almost 7 times more potent toward HDAC6 than toward HDAC1, but is also only a weak inhibitor of HDAC8. However, the inhibition constants are significantly lower than the ones obtained for SAHA. We therefore also tested a second-generation analogue of tubacin, **1**, which can be synthesized using the same methodology as for tubacin. Interestingly, it is found to be 11- and 5-fold more potent than tubacin against HDAC1 and HDAC6, respectively while being only a weak inhibitor of HDAC8.

Although this confirms the previous finding that SAHA is a fairly unselective inhibitor, while tubacin and, to a lesser degree, **1** are class II selective, the measurement of K_i values does not provide the structural insights into the origin of the selectivity that is required for a rational design of isoform-selective inhibitors. We therefore used the methods of molecular docking and molecular dynamics simulation to explain the selectivity of tubacin and **1**, the lack of selectivity in SAHA, and the weak inhibition of HDAC8 by either compound.

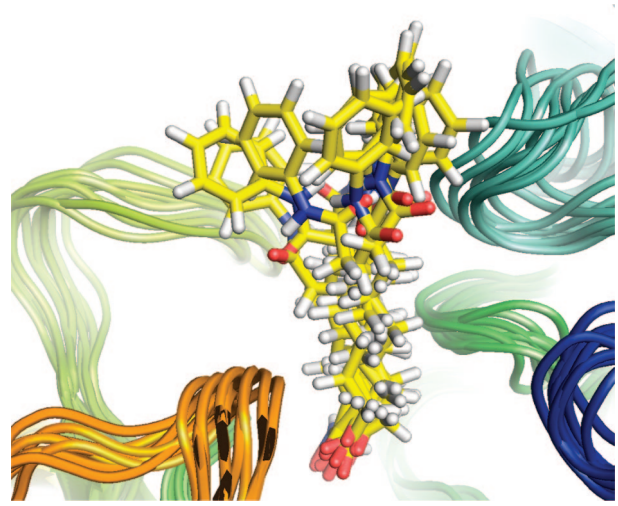

Figure 2. Snapshots from the MD simulation of SAHA in HDAC1.

These questions were addressed using 10 ns molecular dynamics (MD) simulations for each starting structure, built from different orientations of the cap region on the solvent-exposed region of the active site channel. We started our investigations by MD simulations of the best-studied HDAC inhibitor, SAHA. Figure 2 shows a series of snapshots of the simulation of SAHA in HDAC1. As can be seen, no preferred interaction of the cap group on the surface of the protein is found. Rather, SAHA samples the different pockets on the surface of HDAC1 almost equally. The results for HDAC6 and HDAC8 are very similar in that no preferred orientation of the cap group is found (see Figures S1 and S2 in the Supporting Information). This indicates that the interactions in the areas that can be reached by SAHA, which has the smallest of the cap groups studied here, are essentially the same in all directions and in all of the three isoforms studied here.

In the three isoforms, the hydroxamic group is bonded to the zinc ion and the hydrocarbon chain (linker region) fills the narrow portion of the pocket lined by hydrophobic groups (PHE205 and PHE150 in HDAC1). These residues are conserved in the different isoforms, but different interactions of the cap group with residues in the opening of the channel can be distinguished as summarized in the representative snapshots from the simulations shown in Figure 3. For HDAC8, shown on the left, a second PHE group (PHE207) reinforces the lipophilic interaction. This, together with MET274, favors a tilting of the inhibitor to better orient the phenyl moiety toward the lipophilic region of the surface area surrounding the exit of the 11 Å channel. Both the PHE and MET residues are also involved in the stabilization of SAHA in HDAC6, shown in the middle of Figure 3. However, the position of MET184, adjacent to PHE182, does not promote tilting in this structure and does in fact not bind directly to SAHA in any of the snapshots of the simulation shown in the middle of Figure 3. In HDAC1, shown on the right in Figure 3, TYR and PHE residues are involved in the interactions with the cap and the MET274 residue of HDAC8 is replaced by LEU271. The finding that in all three isoforms there is no preferential orientation of

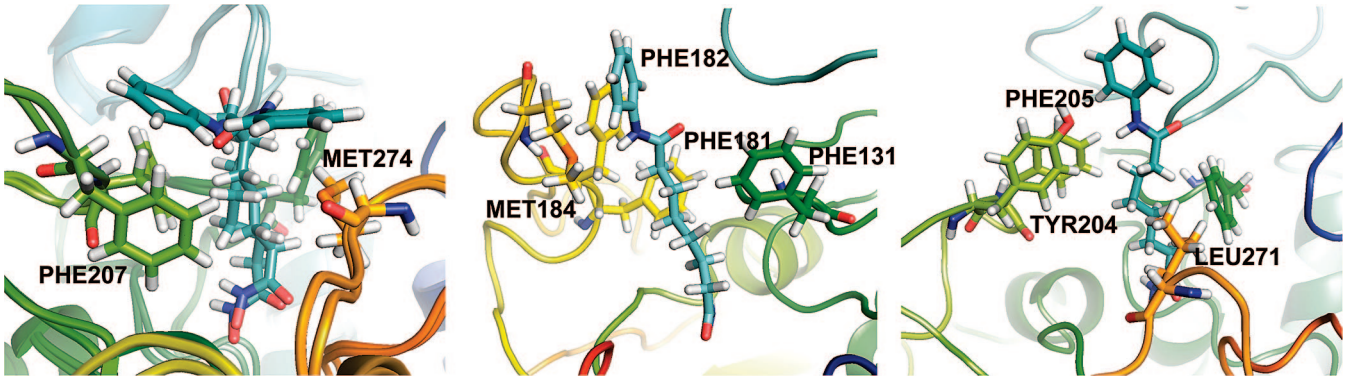

Figure 3. Snapshots from SAHA/HDAC8 simulation with view from surface (left), from SAHA/HDAC6 simulation with view from side of the channel (middle), and from SAHA/HDAC8 simulation with view from side of the channel (right).

the cap group for SAHA indicates that none of the interactions described above are strong enough to provide selective binding to any of the three isoforms studied here, which is in agreement with the experimental observations. This inability of SAHA to distinguish between the surfaces at the active side mouth of the different proteins may result from the small size of the cap group that cannot sample the areas where the overall surface shape (rather than the specific, but similar residues in direct proximity to the 11 Å channel leading to the active site) is different. Similarly, no specific interactions of the phenyl cap group with the protein are found that could favor binding to one of the isoforms over another. These results also show that the experimentally observed poor binding of SAHA to HDAC8 is not a consequence of surface interactions, which are similar between the different isoforms, but rather must be due to changes in the interactions at different parts of the ligand binding site.

We then turned our attention to the structural origin of the selectivity of tubacin, which was identified by screening of a large library of compounds.[13] When the starting geometries were prepared as described above, it was found that several orientations of the cap region were possible. Special care was thus taken to sample a sufficient conformational space for the ligand orientation, and several independent starting geometries were considered for each ligand and each enzyme (this is shown in Figure S3, Supporting Information, for the case of HDAC8 as an example). During the MD simulations, these initial structures converged to two main coordination modes for tubacin for all HDAC isoforms studied here. These and related protein structures remain stable over the 10 ns MD runs with average rmsd values close to 2.1 Å for HDAC8, 2.5 Å for HDAC6, and 3.1 for HDAC1 (Figure S4).

Binding of the hydroxamate moiety to the zinc ion in the active site is consistent with the structures found in earlier docking studies[21] as well as the fact that niltubacin, which lacks this functionality, does not inhibit HDAC6.[13a] As mentioned earlier, these interactions will be very similar for most simple hydroxamates and can therefore not be the reason for the observed selectivity. Rather, the chemical space of the substituents in the cap region, which was sampled in the library screened in the identification of tubacin, has to be responsible for the observed selectivity. Thus, the interactions of this part of the molecule with the residues on the surface of the different isoforms were analyzed in more detail. The results are summarized in Figures 4, 5, and 6, which show snapshots from the MD simulations of tubacin with HDAC6, HDAC1, and HDAC8, respectively.

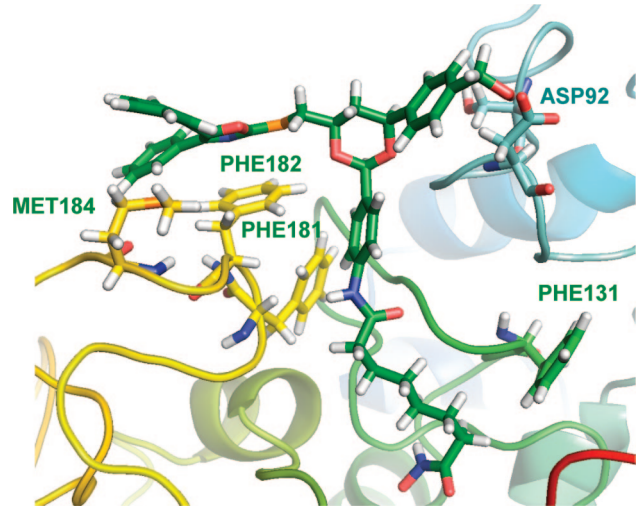

Figure 4. Structure of the HDAC6−tubacin complex that resembles the X-ray-determined structure of FB188-SAHA. Relevant residues are highlighted in yellow (lipophilic) and cyan (hydrophilic).

The coordination modes of HDAC6−tubacin share as a common feature the attachment of the 2,3-diphenyl oxazole moiety to a loop close to the mouth of the active site of the protein that contains the lipohilic residues PHE181 and PHE182 (shown in yellow in Figure 4). The attachment of the diphenyl end of the ligand cap to a lipophilic region of the protein, featured in all the structures after 10 ns MD runs (see Figure S5, Supporting Information for other orientations), highlights the relevance of the lipophilic interactions. It is noteworthy that the shape of the tubacin cap group and the shape of the HDAC6 surface around the active site mouth are complementary and allows simultaneous lipophilic and polar interactions with residues of the two loops, which are stable over the 10 ns MD (see Figure S6, Supporting Information). Other orientations of tubacin toward the 14 Å channel adjacent to the active site that was experimentally found to allow the binding of a second inhibitor molecule[12a] and was hypothesized to be the exit channel for the acetate byproduct[21b] are also possible here as well as in HDAC1 and HDAC8. However, they lead to severe distortions of the ligand and are not consistent with the binding mode observed in the experimental structure of SAHA bound to the bacterial HDAC6 homologue and are thus not considered further.[23a]

The importance of the lipophilic interactions involving the 2,3-diphenyl oxazole moiety of tubacin is also highlighted by the coordination mode obtained from the MD simulations of

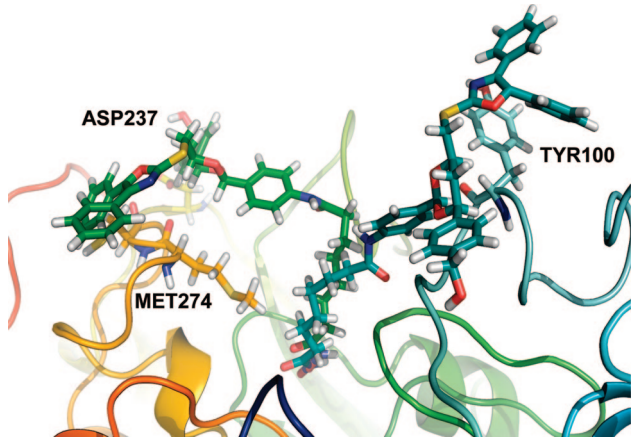

Figure 5. Interactions involved in the HDAC1−tubacin complexes. Relevant residues are highlighted for the most stable interaction mode, shown in green.

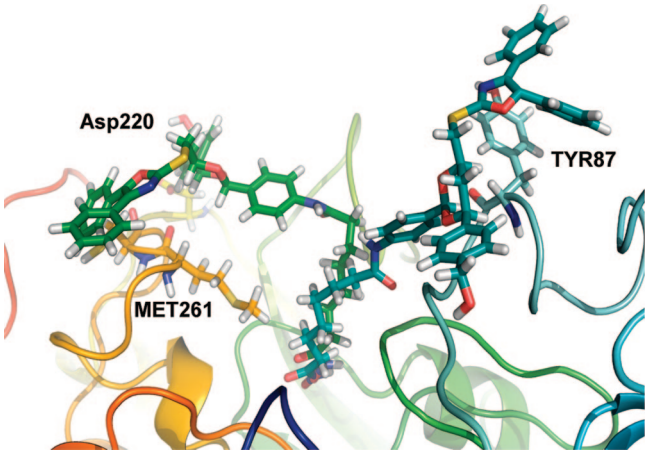

Figure 6. Interactions involved in the stabilization of the HDAC8−tubacin complexes. Relevant residues are highlighted for both coordination modes.

tubacin in HDAC1, shown in Figure 5. In HDAC1, tubacin displays several stable conformations, differentiated by the orientation of the cap moiety in the solvent-exposed surface of the active site channel (Figure S7, Supporting Information). Figure 5 shows in green the orientation most often occupied according to the results of the MD simulations. As was discussed previously, the residues involved in lipophilic interactions are different in HDAC6 and HDAC1. Whereas HDAC6 features PHE and MET residues, HDAC1 has two tyrosine residues in these positions (TYR201, TYR204) that participate in tubacin binding. To allow the interaction with these residues, a tilting of the ligand toward the two tyrosines is necessary. This in turn moves the hydroxymethylphenyl moiety away from the protein into a solvent-exposed position. Unlike the case of HDAC6, a simultaneous interaction with both loops does not appear to be possible due to the difference in the shape of the surfaces of HDAC6 and HDAC1. The analysis of the evolution of the system over 40 ns MD simulations (starting from different configurations) captured several poses with the hydroxymethylphenyl end close to the loop shown in cyan in Figure 5, but they disrupt the interactions with the tyrosines, as shown for one example in Figure 5 in brown. These polar interactions are not strong enough to keep a coordination similar to the one described for HDAC6 because the hydrophobic 2,3-diphenyl oxazole moiety is positioned in an unfavorable solvent-exposed position. Thus, the ligand quickly re-forms the lipophilic interactions in the MD simluation. This effect could potentially be correlated with the experimentally observed lower binding affinity of tubacin to HDAC1 relative to HDAC6. Finally, it should also be pointed out that there are no close contacts with the core dioxane ring of tubacin. This indicates that the identity of this moiety, which was originally chosen based on the ease of synthesis of the library tested, is not important for the activity of tubacin analogues and allows significant structural and stereochemical variation in this core moiety.

The different geometries evaluated for the HDAC8−tubacin complexes also converged to two main conformations after 10 ns MDs that are shown in Figure 6. They feature the ligand tilted toward different sides of the channel in order to allow interactions of the cap with protein residues. Lipophilic interactions with MET274 and CYS275 residues and electronic interaction with ASP237 hold the structure shown in green, whereas lipophilic interactions with TYR100 contribute to the conformation shown in gray, also assisted by polar interactions. However, no conformations where both interactions are intact could be observed during the simulation. No preference for any interaction can be inferred on the basis of X-ray data, as the interaction of either SAHA or MS-344 features a nontilted ligand, which can result from a variety of reasons including the averaging of different geometries and the size of the cap region of the ligands. The evolution of selected distances as a function of time shows that more than 2 ns are necessary to stabilize the structures, as the simulations started from a nontilted geometry of the ligand (Figure S8, Supporting Information). In addition to these geometries, orientations with blockage of the exit channel are also possible for HDAC8 (Figure S9, Supporting Information). As already discussed for the cases of HDAC6 and HDAC1, they lead to severe distortions of the inhibitor and are thus considered to be less favorable.

Comparison of the MD results for the class II and class I HDACs provides insights into the structural origin for the experimentally observed selectivity. Focusing on the interactions of the cap region, the different behavior of tubacin in HDAC6, HDAC1, and HDAC8, respectively, can be explained by three main reasons: First, the shape of the protein surface around the ligand-binding channel is significantly different for class I and class II HDACs. The V-shape of the solvent-exposed surface in HDAC1 or HDAC8, shown in red in Figure 7, is so wide at the top that only one of the two possible contacts between tubacin and the protein surface can occur. In contrast, the solvent-exposed surface in HDAC6, shown in yellow spheres, is narrower and tubacin can simultaneously bind to both sides. Due to the smaller size of the cap group in SAHA, no contacts

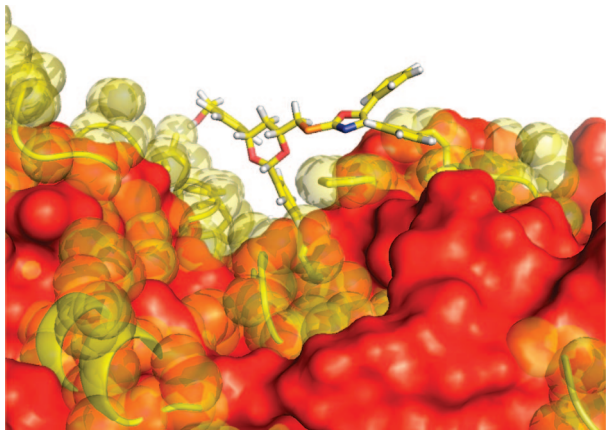

Figure 7. Superposition of HDAC8 (red surface) and HDAC6 (yellow spheres) showing the different shape of the opening of the channel.

are possible on the upper rim of these surfaces. Second, an analysis of the rmsd over the time course of the simulation (see Figure S4, Supporting Information) indicates a lower flexibility of HDAC8 relative to HDAC6 and HDAC1 independent of the ligand studied. Therefore, it appears unlikely that HDAC8 will be able to adjust the overall shape of the surface at the mouth of the active site to allow simultaneous contacts. Finally, the residues in the lipophilic side of the opening of the channel are different between the different isoforms. In this way, the structural characteristics of class II allow tubacin to make good contacts between the cap region and lipophilic and polar residues located in different loops at both sides of the channel. In class I HDACs, on the other hand, interactions with both sides of the channel cannot be established simultaneously, and the ligand has to tilt in one direction for better contact. The results from the simulation of the HDAC1−tubacin complex indicate that the lipophilic interactions are more favorable than the polar ones, leading to a dominance of these conformations.

The different structures of the entrance of the binding channel, together with the lower flexibility of HDAC8, which precludes protein conformational changes to adjust to different ligands, can be used to design HDAC6-selective inhibitors by structural modifications of the cap portion of tubacin. Some of the ligands synthesized and tested by us have increased potency but similar selectivity for HDAC6, An example of such a ligand is **1**, shown in Figure 1, which has a cap region with two lipophilic sides that is thus intermediate between SAHA and tubacin in polarity. If the reasoning outlined above is correct, it should enable us to rationalize the experimentally observed better binding of **1** and potentially derive design motifs for more potent and/or selective inhibitors that could incorporate the favorable interactions obtained in several of these models. We therefore performed MD simulations of the binding of **1** to the three HDAC isoforms studied here, and the results are summarized in Figure 8.

The overall results of the MD simulation on **1** resemble those of tubacin, as is to be expected from the experimentally observed selectivity and similar structure of the two compounds, showing average rms deviations of 2.1, 2.5, and 3.0 for HDAC8, HDAC6, and HDAC1, respectively (see Figure S10). Specifically, **1** makes contacts on both sides of the active site mouth in the case of HDAC6 (shown in Figure 8 left) and to a lesser degree in HDAC1 (Figure 1 middle), but not in HDAC8 (Figure 8 right), in agreement with the argument made above. Interactions with residues of different loops in the protein are also shown in Figure 8 (middle) for the case of HDAC1, rationalizing the higher activity relative to tubacin.

There are also some notable differences that correlate well with the increase in potency of **1**. Analysis of the snapshots and trajectories indicate that the lipophilic interactions in HDAC6−**1** are reinforced by additional nonbonded interactions to the PHE182 and MET184 residues and the 4-thiopyridine moiety of the cap region in **1**. These interactions include both a sulfur−π interaction between both S_1-PHE182 and pyridine$_1$-S-MET184 as well as CH−π contributions between the terminal methyl group of Met184 and the pyridine moiety of **1**. Remarkably, this interaction is strong enough to drive the evolution of the system in the MD simulation from a starting geometry where the S-pyridine end is oriented in opposite direction, toward the protein loop shown in cyan in Figure 6 (see Figure S11, Supporting Information).

Nonbonding sulfur−π interactions with aromatic residues have been discussed previously for stabilizing helical structures and for increasing the association between different subunits in oligomeric proteins.[40] They can involve cystine or methionine sulfur atoms interacting with phenylalanine, histidine, or tyrosine residues. The positioning of a C−H group on top of the N atom of heterocyclic rings, establishing CH−π contributions, has been also observed in the interaction of protein residues with adenine[41] and the indole ring of tryptophane.[42] A statistical analysis of the structures deposited in the Protein Data Bank (as of January 1999) found that 8% of the structures containing a methionine residue interact with an aromatic face (average distance 3.6 A) and 9% are in contact with an aromatic edge (3.7 A).[40a] These interactions are therefore fairly common in determining protein structure, but not been exploited for drug design. Double mutant studies estimated the strength of the sulfur−π interactions to be ∼0.3−0.5 kcal/mol.[40b] The magnitude of the interaction is thus consistent with the experimentally observed binding constant increase between tubacin and **1**. This is to the best of our knowledge the first time such interactions have been realized to be important for the binding of a small molecule ligand to a protein. Because the nonbonded terms in the force field are predominantly parametrized on the basis of empirical data, it is reasonable to expect that they are able to qualitatively reproduce these subtle effects.

In the complex of HDAC6 and **1**, both **1** and the MET sulfur atoms find the appropriate environment, as the **1** sulfur atom can interact with PHE residues of the protein, and the MET thioether with the pyridine end of **1**, as shown in Figure 9 on the left. Time evolution of the interaction over 10 ns, shown in dark blue in Figure 9 on the right, displays different geometries while keeping close contact between MET and the pyridine of **1**, in agreement with this observation. A simultaneous S_1-PHE182/pyridine$_1$-S-MET184 interaction has been observed in several snapshots, but is not stable over the 10 ns MD, as shown in light blue in Figure 9 on the right. Instead, different orientations of MET184 and the sulfur moiety of **1** evolve during the simulation, featuring several interaction geometries. Reinforcing our hypothesis, a second coordination mode has been identified, of low relevance for implying a distorted geometry of the ligand, but having the significance of involving similar nonbonded interactions (see Figure 11, Supporting Information). Moreover, a more detailed inspection of the structures show in Figure 6 shows that S-PHE nonbonding interactions are also involved in the stabilization of the HDAC6−tubacin complex, albeit to a lesser extent. The effect of pyridine substitution increasing the strength of these interactions, together with preliminary results of quantum chemical calculations, points to a relevant role of the CH−π contributions.

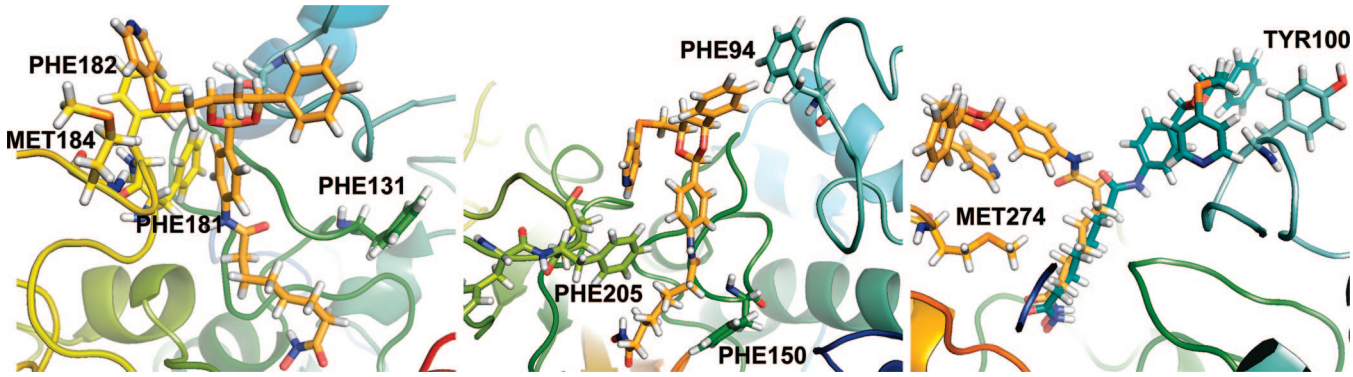

Figure 8. Snapshots from the simulations of **1** with HDAC6 (left), HDAC1 (middle), and HDAC8 (right). Relevant residues are highlighted.

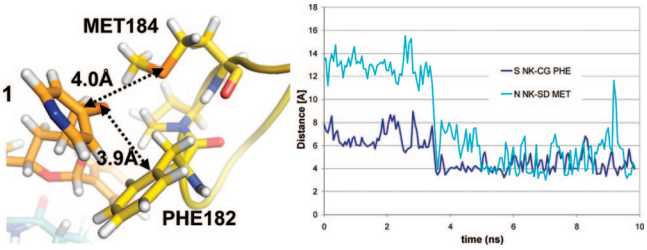

Figure 9. Closeup of the sulfur−π and CH−π interactions in the complex of HDAC6 and **1** (left) and time evolution of key distances over the 10 ns MD simulation (right).

In the case of HDAC1, there is no methionine residue in the lipophilic loop to stabilize similar sulfur−π interactions. Instead, the two lipophilic ends of HDAC6 and **1** can establish simultaneous T-shape and π-stacking interactions with Phe residues of different loops (PHE205, PHE94, respectively, shown in Figure 8, middle) in a way that resembles the coordination in HDAC6. The 4-thiopyridine moiety is significantly smaller than the 2,3-diphenyl oxazole counterpart in tubacin. Therefore, a bending of this moiety leads to T-shape CH−π interactions between the pyridine and PHE205.

The HDAC8−**1** complexes stabilized after 10 ns resemble those described for HDAC8−tubacin (compare Figure 4). Similar to the case of tubacin, **1** can establish only one of the two possible interactions, leading to two possible orientations shown in Figure 8 on the right, where the ligand is tilted to attain additional stabilization through interactions of the cap with protein residues. In addition to the tilting toward the protein, **1** orients the thiopyridine moiety in the conformation shown in orange in Figure 8, middle. The analysis of the distances to the residues in the vicinity shows a preference for the interaction with MET274, with a competition between the pyridine and the phenyl groups adjacent to the linker region for its stabilization (Figure S12, Supporting Information). This conformation also favors a hydrogen-bond-type interaction with an adjacent CYS. As for the case of tubacin, the coordination of **1** shown in cyan in Figure 8 (right) is mainly stabilized by lipophilic interactions with TYR100, keeping the pyridine end close to PRO103 (Figure S11, Supporting Information).

Conclusions

The experimentally determined differences in binding constants of the class II-selective ligands tubacin and **1** can be elucidated by comparison with SAHA, which was found to be unselective with respect to the class 1 isoform HDAC1 and the class IIb HDAC6, but has a much lower activity toward HDAC8. The analysis of the MD results points to the opening of the active site as the region of focus in order to design modifications oriented to improve isoform selectivity. Interactions with this region are mainly of lipophilic and/or nonbonded nature and are more efficiently established in the narrower pocket of HDAC6. The different structural characteristics and shape of the protein surface around the ligand-biding site and, to a lesser degree, the differences in protein flexibility between HDAC6 and HDAC8 thus evolve as the key determinant for the rational design of class II vs class I selective HDAC inhibitors.

In addition to the results rationalizing the experimentally observed selectivities, the MD simulations also uncovered several nonbonded contacts that have not been described before in HDAC inhibitor complexes and could potentially be used to improve the potency of novel HDAC inhibitors. Specifically, the polar contacts of the aspartate residue on the polar loop as well as a sulfur−π interaction that has to the best of our knowledge not previously been exploited for drug design are able to increase the binding constants of novel inhibitors. The design, synthesis, and evaluation of novel HDAC inhibitors that make use of these principles is currently in progress.

While these design elements for the cap region are useful, other recent results from our group[43] and others[44] indicate that the linker region is also important for the binding of substrate and ligands. Finally, the overall low susceptibility of HDAC8 toward inhibition by the ligands discussed here indicates that other factors specific to HDAC8 make this a poor model of other class 1 HDACs, as is reflected by the weak phylogenetic relation of HDAC8 to HDAC1.[11] The fact that the surface interactions of SAHA are very similar in all three isoforms studied here indicates that other factors must be responsible for the weak inhibition of HDAC8 by SAHA.

Acknowledgment. We thank the Walther Cancer Institute (G. E. and O.W.), the Multiple Myeloma Research Foundation (J.E.B. and E.F.G), and the National Cancer Institute Initiative for Chemical Genetics (R.M.) for support of this research. Generous allocation of computing resources by the Center for Research Computing at the University of Notre Dame is also gratefully acknowledged.

Supporting Information Available: Rmsd plots and simulation snapshots as well as coordinates of tubacin in HDAC1, -6, and -8 (pdb format) are available free of charge via the Internet at http://pubs.acs.org. Additional structures of the HDAC inhibitor complexes are available from the authors upon request.

References

(1) (a) Baylin, S. B.; Ohm, J. E. Epigenetic gene silencing in cancer: a mechanism for early oncogenic pathway addiction. *Nature Rev. Cancer* **2006**, *6*, 107–116. (b) Xu, W. S.; Parmigiani, R. B.; Marks, P. A.

Histone deacetylase inhibitors. Molecular mechanisms of action. *Oncogene* **2007**, *26*, 5541–5552.
(2) Lund, A. H.; van Lohuizen, M. Epigenetics and cancer. *Genes Dev.* **2004**, *18*, 2315–2335.
(3) Bolden, J.; Peart, M.; Johnstone, R. Anticancer activities of histone deacetylase inhibitors. *Nature* **2006**, *5*, 769–784.
(4) (a) Roth, S. Y.; Denu, J. M.; Allis, C. D. Histone acetyltransferases. *Annu. Rev. Biochem.* **2001**, *70*, 81–120. (b) Hodawadekar, S. C.; Marmorstein, R. Chemistry of acetyl transfer by histone modifying enzymes: structure, mechanism and implications for effector design. *Oncogene* **2007**, *26*, 5528–5540.
(5) Thiagallingam, S. Histone deacetylases: unique players in shaping the epigenetic histone code. *Annu. NY Acad. Sci.* **2003**, *983*, 84–100.
(6) Rosato, R. R.; Grant, S. Histone deacetylase inhibitors in cancer therapy. *Cancer Biol. Ther.* **2003**, *2*, 30–37.
(7) Villar-Garea, A.; Esteller, M. Histone deacetylase inhibitors: understanding a new wave of anticancer agents. *Int. J. Cancer* **2004**, *112*, 171–178.
(8) Jabbour, E. J.; Giles, F. J. New agents in myelodysplastic syndromes. *Curr. Hematol. Rep* **2005**, *4*, 191–199.
(9) Lindemann, R. K.; Gabrielli, B. Histone deacetylase inhibitors for the treatment of cancer. Johnstone, R. W. *Cell Cycle* **2004**, *3*, 779–788.
(10) Marks, P.; Jiang, X. Histone deacetylese inhibitors in programmed cells death and cancer therapy. *Cell Cycle* **2005**, *4*, 549–551.
(11) Gregoretti, I.; Lee, Y. -M.; Goodson, H. V. Molecular evolution of the histone deacetylase family: Functional implications of phylogenetic analysis. *J. Mol. Biol.* **2004**, *338*, 17–31.
(12) (a) Bhalla, K. N. Epigenetic and chromatin modifiers as targeted therapy of hematologic malignancies. *J. Clin. Oncol.* **2005**, *23*, 3971–3993.
(13) (a) Haggarty, S. J.; Koeller, K. M.; Wong, J. C.; Grozinger, G. M.; Schreiber, S. L. Domain selective small molecule inhibitor of histone deacetylase 6 (HDAC6) mediated tubulin deacetylation. *Proc. Natl. Acad. Sci.* **2003**, *100*, 4389–4394. (b) Hideshima, T.; Bradner, J. E.; Wong, J.; Chauhan, D.; Richardson, P.; Schreiber, S. L.; Anderson, K. C. Small-molecule inhibition of proteasome and aggresome function induces synergistic antitumor activity in multiple myeloma. *Proc. Natl. Acad. Sci.* **2005**, *102*, 8567–8572. (c) Santander, V. S.; Bisig, C. G.; Purro, S. A.; Casale, C. H.; Arce, C. A.; Barra, H. S. Tubulin must be acetylated in order to form a complex with membrane Na+,K+-ATPase and to inhibit its enzyme activity. *Mol. Cell. Biochem.* **2006**, *91*, 167–174. (d) Cabrero, J. R.; Serrador, J. M.; Barreiro, O.; Mittelbrunn, M.; Naranjo-Suarez, S.; Martin-Cofreces, N.; Vicente-Manzanares, M.; Mazitschek, R.; Bradner, J. E.; Avila, J.; Valenzuela-Fernandez, A.; Sanchez-Madrid, F. Lymphocyte chemotaxis is regulated by histone deacetylase 6, independently of Its deacetylase activity. *Mol. Biol. Cell* **2006**, *17*, 3435–3445. (e) Tran, A. D.; Marmo, T. P.; Salam, A. A.; Che, S.; Finkelstein, E.; Kabarriti, R.; Xenias, H. S.; Mazitschek, R.; Hubbert, C.; Kawaguchi, Y.; Sheetz, M. P.; Yao, T. P.; Bulinski, J. C. HDAC6 deacetylation of tubulin modulates dynamics of cellular adhesions. *J. Cell Sci.* **2007**, *120*, 1469–1479.
(14) Hildmann, C.; Wegener, D.; Riester, D.; Hempel, R.; Schober, A.; Merana, J.; Giurato, L.; Guccione, S.; Nielsen, T. K.; Ficner, R.; Schwienhorst, A. Substrate an inhibitor specificity of class 1 and class 2 histone deacetylases. *J. Biotechnol.* **2006**, *124*, 258–270.
(15) Park, J. H.; Jung, Y.; Kim, T.; Kim, S.; Jong, H.-S.; Lee, J. W.; Kim, D.-K.; Lee, J.-S.; Kim, N. K.; Kim, T.-Y.; Bang, Y.-J. Class 1 histone deacetylase-selective novel synthetic inhibitors potently inhibit human tumor proliferation. *Clin. Cancer Res.* **2004**, *10*, 5271–5281.
(16) Furumai, R.; Komatsu, Y.; Nishino, N.; Khochbin, N.; Yoshida, M.; Horinouchi, S. Potent histone deacetylase inhibitors built from trichostatin A and cyclic tetrapeptide antibiotics including trapoxin. *Proc. Natl. Acad. Sci. U.S.A.* **2001**, *98*, 87–92.
(17) (a) Kawaguchi, Y.; Kovacs, J.; McLaurin, A.; Vance, J. M.; Ito, A.; Yao, T. P. The deacetylase HDAC6 regulates aggresome formation and cell viability in response to misfolded protein stress. *Cell* **2003**, *115*, 727–738. (b) Yang, X.-J.; Gregoire, S. Class II Histone Deacetylases: from Sequence to Function, Regulation, and Clinical Implication. *Mol. Cell. Biol.* **2005**, *25*, 2873–2884. (c) Boyault, C.; Sadoul, K.; Pabion, M.; Khochbin, S. HDAC6, at the crossroads between cytoskeleton and cell signaling by acetylation and ubiquitination. *Oncogene* **2007**, *26*, 5468–5476.
(18) Barnes, D. W.; Koehler, A. N.; Bradner, J. E.; Mazitschek, R.; Schreiber, S. L. Small molecule printing using compounds and methods to identify compounds that interact with a biological macromolecule. Patent WO2008013569.
(19) Wang, D.-F; Wiest, O.; Helquist, P. Zinc binding in HDAC inhibitors. A DFT study. *J. Org. Chem.* **2007**, *72*, 5446–5449.
(20) (a) Vanommeslaeghe, K.; Van Alsenoy, C.; De Proft, F.; Martins, J. C.; Tourwé, D.; Geerlings, P. Theoretical study revealing the functioning of a novel combination of catalytic motifs in histone deacetylase. *Org. Biomol. Chem.* **2003**, *1*, 2951–2957. (b) Vanommeslaeghe, K.; De Proft, F.; Loverix, S.; Tourwé, D.; Geerlings, P. DFT-based ranking of zinc-binding groups in histone deacetylase inhibitors. *Bioorg. Med. Chem.* **2005**, *13*, 3987–3992. (c) Vanommeslaeghe, K.; Loverix, S.; Geerlings, P.; Tourwé, D. Ab initio study of the binding of trichostatin A (TSA) in the active site of histone deacetylase like Protein (HDLP). *Bioorg. Med. Chem.* **2005**, *13*, 6070–6082.
(21) (a) Somoza, J. R.; Skene, R. J.; Katz, B. A.; Moi, C.; Ho, J. D.; Jennings, A. J.; Luong, C.; Arvai, A.; Buggy, J. J.; Chi, E.; Tang, J.; Sang, B. C.; Verner, E.; Wynands, R.; Leahy, E. M.; Dougan, D.; Snell, G.; Navre, M.; Knuth, M. W.; Swanson, R. V.; McRee, D.; Tari, L. W. Structural snapshots of Human HDAC8 provide Insights into Class I Histone Deacetylases. *Structure* **2004**, *12*, 1325–1334. (b) Vannini, A.; Volpari, C.; Filocamo, G.; Caroli Casavola, E.; Brunetti, M.; Renzoni, D.; Chakravarty, P.; Paolini, C.; De Francesco, R.; Gallinari, P.; Steinckuhler, C.; Di Marco, S. Crystal structure of a eukariotic zinc-dependent histone deacetylase, human HDAC8, complexed with a hydroxamic acid inhibitor. *Proc. Natl. Acad. Sci. U.S.A.* **2004**, *101*, 15064–15069. Compare also the structure of the histone deacetylase-like protein (HDLP): (c) Finnin, M. S.; Donigian, J. R.; Cohen, A.; Richon, V. M.; Rifkind, R. A.; Marks, P. A.; Breslow, R.; Pavletich, N. P. Structure of histone deacetylase homologue bound to the TSA and SAHA inhibitors. *Nature* **1999**, *401*, 188–193.
(22) (a) Nielsen, T. K.; Christian, H.; Dickmanns, A.; Schwienhorst, A.; Ficner, R. Crystal structure of a bacterial class 2 histone deacetylase homologue. *J. Mol. Biol.* **2005**, *354*, 107–120, Note that two structures of a human class IIa HDAC have been recently deposited in the PDB under pdb codes 2pqo and 2pqp. (b) Schuetz, A., Min, J., Loppnau, P.; Weigelt, J.; Sundstrom, M.; Arrowsmith, C. H., Edwards, A. M.; Bochkarev, A.; Plotnikov, A. N. To be published.
(23) (a) Wang, D.-F.; Wiest, O.; Helquist, P.; Lan-Hargest, H.-Y.; Wiech, N. L. Toward selective histone deacetylase inhibitor design. Homology modeling, docking studies and molecular dynamic simulations of human class I histone deacetylases. *J. Med. Chem.* **2004**, *47*, 3409–3417. (b) Wang, D.-F.; Wiest, O.; Helquist, P.; Wiech, N. L. On the function of the 14 A long internal cavity of histone deacetylase-like protein: Implications for the design of histone deacetylase inhibitors. *J. Med. Chem.* **2005**, *48*, 6936–6947.
(24) (a) Altschul, S. F.; Gish, W.; Miller, W.; Myers, E. W.; Lipman, D. J. Basic local alignment search tool. *J. Mol. Biol.* **1990**, *215*, 403–410. (b) Altschul, S. F.; Madden, T. L.; Schäffer, A. A.; Zhang, J.; Zhang, Z.; Miller, W.; Lipman, D. J. Gapped BLAST and PSI-BLAST: a new generation of protein database search programs. *Nucleic Acids Res.* **1997**, *25*, 3389–3402. (c) Schäffer, A. A.; Aravind, L.; Madden, T. L.; Shavirin, S.; Spouge, J. L.; Wolf, Y. I.; Koonin, E. V.; Altschul, S. F. Improving the accuracy of PSI-BLAST protein database searches with composition-based statistics and other refinements. *Nucleic Acids Res.* **2001**, *29*, 2994–3005.
(25) (a) Fiser, A.; Do, R. K.; Sali, A. Modeling of loops in protein structures. *Protein Sci.* **2000**, *9*, 1753–1773. (b) Marti-Renom, M. A.; Stuart, A.; Fiser, A.; Sánchez, R.; Melo, F.; Sali, A. Comparative protein structure modeling of genes and genomes. *Annu. Rev. Biophys. Biomol. Struct.* **2000**, *29*, 291–325. (c) Sali, A.; Blundell, T. L. Comparative protein modelling by satisfaction of spatial restraints. *J. Mol. Biol.* **1993**, *234*, 779–815.
(26) (a) Laskowski, R. A.; MacArthur, M. W.; Moss, D. S.; Thornton, J. M. PROCHECK: a program to check the stereochemical quality of protein structures. *J. Appl. Crystallogr.* **1993**, *26*, 283–291. (b) Morris, A. L.; MacArthur, M. W.; Hutchinson, E. G.; Thornton, J. M. Stereochemical quality of protein structure coordinates. *Proteins* **1992**, *12*, 345–364.
(27) McLachlan, A. D. Rapid comparison of protein structures. *Acta Crystallogr.* **1982**, *A38*, 871–873.
(28) Jorgensen, W. L.; Madura, J.; Impey, R. W.; Klein, M. L. Comparison of simple potential functions for the simulation of liquid water. *J. Chem. Phys.* **1983**, *79*, 926–935.
(29) Schafmeister, C.; Ross, W. S.; Romanovski, V. *LEaP*, University of California: San Francisco, 1995.
(30) Cieplak, P.; Caldwell, J.; Kollman, P. A. Molecular mechanical models for organic and biological systems going beyond the atom centered two body additive approximation: Aqueous solution free energies of methanol and N-ethyl acetamide, nucleic acid base, and amide hydrogen bonding and chloroform/water partition coefficients of the nucleic acid bases. *J. Comput. Chem.* **2001**, *22*, 1048–1057.
(31) (a) Wang, J.; Wang, W.; Kollman, P. A.; Case, D. A. Automatic atom type and bond type perception in molecular mechanical calculations. *J. Mol. Graph. Mod.* **2006**, *25*, 247–260. (b) Wang, J.; Wolf, R. M.; Caldwell, J. W.; Kollman, P. A.; Case, D. A. Development and testing of a general AMBER force field. *J. Comput. Chem.* **2004**, *25*, 1157–1174.
(32) (a) Bayly, C. A.; Cieplak, P.; Cornell, W. D.; Kollman, P. A. A well behaved elestrostatic potential based method using charge restraints for deriving atomic charges: The RESP model. *J. Phys. Chem.* **1993**, *97*, 10269–10280. (b) Pearlman, D. A.; Case, D. A.; Caldwell, J. W.; Ross, W. S.; Cheatham, T. E.; Debolt, S.; Ferguson, D.; Seibel, G.; Kollman, P. A. AMBER, a package of computer programs for applying

molecular mechanics, normal mode analysis, molecular dynamics and free energy calculations to simulate the structural and energetic properties of molecules. *Comput. Phys. Commun.* **1995**, *91*, 1–41. (c) Fox, T.; Kollman, P. A. Application of RESP methodology in the parametrization of organic solvents. *J. Phys. Chem. B* **1998**, *102*, 8070–8079.

(33) Case, D. A.; Darden, T. A.; Cheatham, T. E.; Simmerling, C. L.; Wang, J.; Duke, R. E.; Luo, R.; Merz, K. M.; Wang, B.; Pearlman, D. A.; Crowley, M.; Brozell, S.; Tsui, V.; Gohlke, H.; Mongan, J.; Hornak, V.; Cui, G.; Beroza, P.; Schafmeister, C.; Caldwell, J. W.; Ross, W. S.; Kollman, P. A., *AMBER 8*; University of California: San Francisco, CA, 2004.

(34) Ryckaert, J. P.; Ciccotti, G.; Berendsen, H. J. C. Numerical integration of the cartesian equations of motion of a system with constraints: Molecular dynamics of n-alkanes. *J. Comput. Phys.* **1977**, *23*, 327–341.

(35) (a) Berendsen, H. J. C.; Potsma, J. P. M.; van Gunsteren, W. F.; DiNola, A. D.; Haak, J. R. Molecular dynamics with coupling to an external bath. *J. Chem. Phys.* **1984**, *81*, 3684–3690. (b) van Gunsteren, W. F.; Berendsen, H. J. C. Algorithm for macromolecular dynamics and constraint dynamics. *Mol. Phys.* **1977**, *34*, 1311–1327.

(36) (a) Essman, V.; Perera, L.; Berkowitz, M. L.; Darden, T.; Lee, H.; Pedersen, L. G. A smooth particle-mesh-Ewald method. *J. Chem. Phys.* **1995**, *103*, 8577–8593. (b) Petersen, L. G. Accuracy and efficiency of the particle-mesh-Ewald method. *J. Chem. Phys.* **1995**, *103*, 3668–3679.

(37) Kapustin, G. V.; Fejer, G.; Gronlund, J. L.; McCafferty, D. G.; Seto, E.; Etzkorn, F. A. Phosphorus-based SAHA analogues as histone deacetylase inhibitors. *Org. Lett.* **2003**, *5*, 3053–3056.

(38) Khan, N.; Jeffers, M.; Kumar, S.; Hackett, C.; Boldog, F.; Khramtsov, N.; Qian, X.; Mills, E.; Berghs, S. C.; Carey, N.; Finn, P. W.; Collins, L. S.; Tumber, A.; Ritchie, J. W.; Jensen, P. B.; Lichenstein, H. S.; Sehested, M. Determination of the class and isoform selectivity of small-molecule histone deacetylase inhibitors. *Biochem. J.* **2008**, *409*, 581–589.

(39) KrennHrubec, K.; Marshall, B. L.; Hedglin, M.; Verdin, E.; Ulrich, S. M. Design and evaluation of linkerless hydroxamates as selective HDAC8 inhibitors. *Bioorg. Med. Chem.* **2007**, *17*, 2874–2878. (b) Waltregny, D.; De Leval, L.; Glenisson, W.; Ly Tran, S.; North, B. J.; Bellahcene, A.; Weidle, U.; Verdin, E.; Castronovo, V. Expression of histone deacetylase 8, a class I histone deacetylase, is restricted to cells showing smooth muscle differentiation in normal human tissues. *Am. J. Pathol.* **2004**, *165*, 553–564. (c) Waltregny, D.; Glenisson, W.; Tran, S. L.; North, B. J.; Verdin, E.; Colige, A.; Castronovo, V. Histone deacetylase HDAC8 associates with smooth muscle {alpha}-actin and is essential for smooth muscle cell contractility. *FASEB J.* **2005**, *19*, 966–968.

(40) (a) Pal, D.; Chakrabarti, P. Non-hydrogen bond interaction involving the methionine sulfur atom. *J. Biomol. Struct. Dyn.* **2001**, *19*, 115–128. (b) Tatko, C.; Waters, M. Investigation of the nature of the π/methionine interaction in beta hairpin peptide model systems. *Protein Sci.* **2004**, *13*, 2515–2522. (c) Ringer, A. L.; Senenko, A.; Sherill, C. D. Models of S/π interactions in protein structures: Comparison of the H2S-benzene complex with PDB data. *Protein Sci.* **2007**, *16*, 2216–2223.

(41) Chakrabarti, P.; Samanta, U. CH/pi Interaction in the Packing of the Adenine Ring in Protein Structures. *J. Mol. Biol.* **1995**, *251*, 9–14.

(42) Samanta, U.; Pal, D.; Chakrabarti, P. Environment of tryptophan side chains in proteins. *Proteins* **2000**, *38*, 288–300.

(43) Weerasinghe, S. V. W.; Estiu, G.; Wiest, O.; Pflum, M. K. H., submitted for publication.

(44) (a) Simonini, M. V.; Camargo, L. M.; Dong, E.; Maloku, E.; Veldic, M.; Costa, E.; Guidotti, A. From the Cover: The benzamide MS-275 is a potent, long-lasting brain region-selective inhibitor of histone deacetylases. *Proc. Natl. Acad. Sci. U.S.A.* **2006**, *103*, 1587–1592. (b) Hess-Stumpp, H.; Bracker, T. U.; Henderson, D.; Politz, O. MS-275, a potent orally available inhibitor of histone deacetylases—The development of an anticancer agent. *Int. J. Biochem. Cell Biol.* **2007**, *39*, 1388–1405.

JM7015254